Absence of volume metastability in bcc copper

Z. W. Lu, S.-H. Wei, and Alex Zunger
Solar Energy Research Institute, Golden, Colorado 80401
(Received 28 August 1989)

A previous pseudopotential total-energy calculation on bcc copper revealed a structural metastability in the form of a double-well total-energy curve with two local minima (at 6% compression and 7% dilation relative to the observed equilibrium volume of the fcc structure), separated by a barrier. This was explained in terms of a symmetry breaking in the nonspherical components of the valence-electron charge density upon volume change. Our present all-electron calculation shows no such metastability; analysis of the response of the valence-electron charge density to volume deformations indeed shows no cause for such a metastability.

I. INTRODUCTION

Kang, Tartar, Mele, and Soven[1] (KTMS) developed a mixed-basis approach to the band-structure problem in which the wave function is expanded in plane waves plus a set of nonoverlapping (numerically integrated) radial atomic orbitals. Unlike an earlier mixed-basis approach,[2] they used a pseudopotential to replace the all-electron potential. As a test case, they applied the new method to calculate the electronic properties of face-centered-cubic (fcc) and body-centered-cubic (bcc) copper. Their calculated total-energy curves, obtained by extending the convergence parameter of the method so that a nominal stability of 0.01 mRy is obtained, is shown in Fig. 1(a). For fcc Cu they find an equilibrium lattice constant and bulk modulus in reasonable accord with experiment[3] and with previous KKR (Ref. 4) (Korringa-Kohn-Rostoker) and ASW (Refs. 5 and 6) (augmented-spherical-wave) calculations. However, for bcc Cu they unexpectedly[1] find a double-well total-energy curve with minima at $V/V_0=1.07$ and 0.94, where $V_0=7.083$ cm^3/g-at. is the experimentally observed equilibrium molar volume of Cu. KTMS analyzed this anomaly in terms of the valence-electron pseudo-charge-density $\rho(\mathbf{r})$ and concluded that the anomaly reflects the different response of the nonspherical pieces of $\rho(\mathbf{r})$ in bcc and fcc Cu to volume change. It was argued[1] that since earlier published calculations[4-6] invoked spherical approximations to the charge density and potential, they could have missed this effect. Later on, Chelikowsky and Chou[7] have used a Gaussian-basis-set approach with a smoothed Cu pseudopotential (different from that used in Ref. 1), finding good agreement with the results of KTMS for fcc Cu, but failing to reproduce their unusual results for bcc Cu. Morrison, Kang, and Mele[8] have subsequently repeated the calculation of Ref. 1 using a lower-symmetry unit cell, again finding the same double-well metastability in bcc Cu. They raised, however, the possibility that the difference between their calculation and that of Chelikowsky and Chou[7] might represent a computational difficulty in accurately representing, within their plane-wave expansion, the short-wavelength near-core changes in the charge density attendant upon compression.

In an attempt to resolve the issue of existence or nonexistence of metastable bcc Cu, and the broader question of the role of nonspherical charge-density components in the phase stability of Cu, we have repeated the calculations of Refs. 1 and 4–8 using an all-electron band-structure technique which retains the full nonspherical components of the valence-electron charge density

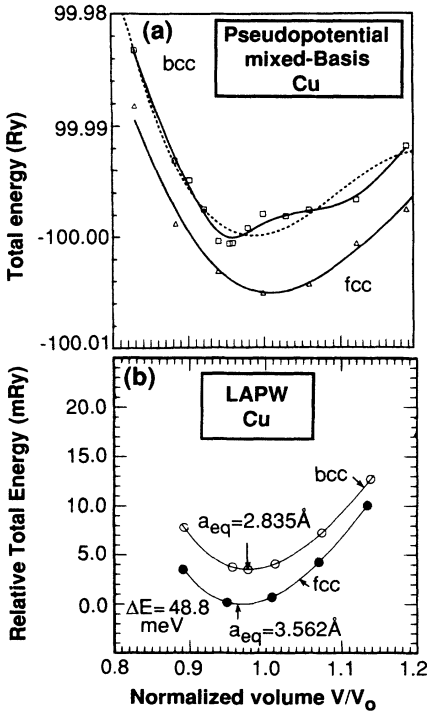

FIG. 1. (a) Total-energy curves for fcc and bcc Cu from Ref. 8 (see also Ref. 1) obtained from a mixed-bases pseudopotential calculation, showing the double-minimum metastability for bcc Cu. (b) Results of the present all-electron LAPW calculation, showing smooth total-energy curves for both fcc and bcc structures.

and involves a robust representation of short-wavelength charge fluctuations. Specifically, we use the general potential linear augmented-plane-wave (LAPW) method[9] within the Hohenberg-Kohn-Sham local-density approximation (LDA),[10] and the Wigner form[11] of the exchange-correlation potential. We do not find any structure metastability in bcc Cu; analysis of the volume deformations in the nonspherical charge density suggests that no metastability is to be expected.

II. CALCULATION

A semirelativistic Hamiltonian is used for the valence-electron states, whereas the core states ($1s$–$3p$) are treated fully relativistically in a spherical, self-consistent potential. The muffin-tin (MT) radii are chosen to be 2.2 a.u. = 1.164 Å for both fcc and bcc Cu. The cutoff kinetic energy for the LAPW basis-set expansion is 16.7 Ry; it is kept fixed for all calculations. Inside the MT sphere the nonspherical charge and potential are expanded in terms of lattice harmonics $K_l(\hat{\mathbf{r}})$ of angular momentum $l \leq 8$: For the charge density it reads

$$\rho(\mathbf{r}) = \rho_0(|\mathbf{r}|) + \sum_{l\,(\neq 0)} \rho_l(|\mathbf{r}|) K_l(\hat{\mathbf{r}}), \quad \mathbf{r} \in \mathrm{MT} . \tag{1}$$

The first term represents the spherical density about a given atom, while the second term gives the nonspherical (NS) charge density $\rho_{\mathrm{NS}}(\mathbf{r})$. By symmetry, the lattice harmonics of the fcc and bcc lattices are identical: both contain the same $l=4$, 6, and 8 terms. In the interstitial (I) region, between the MT spheres, we use a symmetrized-plane-wave representation

$$\rho(\mathbf{r}) = \sum_s \rho_s \phi_s(\mathbf{r}), \quad \mathbf{r} \in I , \tag{2}$$

where $\phi_s(\mathbf{r})$ are symmetrized plane waves ("star functions"). The expansion coefficients ρ_l and ρ_s are determined variationally from a Brillouin-zone sum of the amplitudes of the self-consistent wave functions whose energy is below the Fermi surface. Sixty and forty special-**k** points[12] are used for the Brillouin-zone integration over an irreducible wedge for the fcc and bcc structure, respectively. The calculated charge density is continuous and smooth across the MT boundaries. The total energy of the Cu atom is calculated in a $d^{10}s^1$ configuration, to which we add a spin-polarization energy[13] of -0.27 eV. With these convergence parameters, the cohesive energy is converged to about 0.5 mRy.

III. RESULTS

Our calculated total-energy curves [Table I (Refs. 14–16) and Fig. 1(b)] are regular and smooth for both fcc and bcc Cu; no metastability is found in bcc Cu, in agreement with Chelikowsky and Chou,[7] but in disagreement with KTMS (Ref. 1) and with Morrison *et al.*,[8] suggesting a possible computational error in the latter calculations.[1,8]

Our results agree reasonably well with previous published data[1,4–8] on fcc Cu (Table I); the all-electron equilibrium lattice constants are, however, systematically smaller than the pseudopotential values, and the cohesive energies are >0.5 eV larger. Interestingly, Table I shows that a nonrelativistic (NR) calculation produces better agreement with measured structural and cohesive properties than a semirelativistic (SR) calculation; the latter tends to produce smaller lattice constants and larger bulk moduli and cohesive energies. The reduction in the cohesive energy in the nonrelativistic calculation is par-

TABLE I. Calculated structural and cohesive properties of fcc and bcc copper. Lattice constants a in Å, bulk moduli B in Mbar, and cohesive energies E_c in eV. For the present all-electron calculation, we present both semirelativistic (SR) and nonrelativistic (NR) results. $\Delta E = E_{\mathrm{bcc}} - E_{\mathrm{fcc}}$ (in units of meV) is the bcc-fcc energy difference taken at the respective calculated equilibrium lattice constants.

	Pseudopotential mixed basis[a]	KKR[b]	ASW[c]	ASW[d]	Pseudopotential Gaussian[e]		All electron[g]	
	SR	NR	NR	SR	SR	Expt.[f]	SR	NR
a(fcc) (Å)	3.62	3.58	3.61	3.55	3.62	3.61	3.56	3.61
a(bcc) (Å)	2.81, 2.93		2.87		2.87		2.84	2.86
B(fcc) (Mbar)	1.50	1.52	1.29	1.86	1.88	1.42	1.83	1.62
B(fcc) (Mbar)					1.85		1.79	1.60
E_c(fcc) (eV)	3.35	4.10	2.98		3.83	3.50	4.42	4.14
E_c(bcc) (eV)			~ 2.97		3.81		4.37	4.12
ΔE (meV)	41.0		<10.0		20.0		48.8	17.7

[a]Reference 1, using Ceperley-Adler exchange-correlation (xc) potential (Ref. 14), parameterized by Perdew and Zunger (Ref. 15).
[b]Reference 4, using a modified Hedin-Lundqvist (HL) xc potential, Ref. 16.
[c]Reference 5, using the same xc potential as in Ref. 4.
[d]Reference 6, using the same xc potential as in Ref. 4.
[e]Reference 7 using the HL xc potential.
[f]Reference 3.
[g]Present result, using the Wigner exchange-correlation potential, Ref. 11, and 60 (40) **k** points for fcc (bcc). Using only 10 **k** points (Ref. 13) gives for fcc $a=3.577$ Å, $B=1.44$ Mbar, and $E_c=4.33$ eV.

ticularly dramatic in metals whose s- to d-electron ratio is small, e.g., in fcc Pd a relativistic calculation gives $E_c=5.05$ eV, while a nonrelativistic calculation gives 3.95 eV (the observed value is 3.89 eV). This reflects the changed occupation of s-like wave functions in the solid relative to the free atom: The relativistic lowering of the total energy is proportional to the s-electron content of the system (since the s states have the largest weight around the nuclei). This lowering $E^{NR}-E^{SR}$ is smaller in the Cu $d^{10}s^1$ or Pd $d^{10}s^0$ *free atoms* than in the respective *solids,* where the ground state contains more s character (a hybridization effect). This reduces E_c^{NR} relative to E_c^{SR}. These large errors largely reflect LDA errors in the *atoms.* In general, we find that quantities which do not involve directly atomic properties (bulk moduli, equilibrium lattice constants) exhibit smaller LDA errors in the $4d$ row than in the $3d$ row, e.g., for Pd we find $a=3.882$ Å (versus 3.887 Å, measured) and $B=2.11$ Mbar (versus 1.94 Mbar, measured).

IV. ANALYSIS OF THE CHARGE-DENSITY RESPONSE TO VOLUME CHANGES

We next proceed to the analysis of our results in terms of the deformation valence-electron charge densities, as suggested by KTMS.

Figures 2(a) and 2(b) depict the *total* valence-electron charge densities in fcc copper [2(a), at the experimental equilibrium lattice constant] and bcc copper [2(b), at the calculated equilibrium lattice constant]; only bands above Cu $3p$ are included in these plots. Both charge densities appear similar as they are equally dominated by the spherical component [ρ_0 in Eq. (1)]. The differences in the interstitial regions (shaded) reflect the smaller interstitial space in the fcc lattice: a larger fraction of the cell volume is occupied by touching spheres in a fcc cell (74.0%) than in a bcc cell (68.0%). [A comparison of the symmetries and dimensions of $\rho(\mathbf{r})$ in Fig. 2 to the analogous quantities plotted by KTMS (Ref. 1) shows that they have mislabeled their Fig. 5 as fcc (which should be bcc) and their Fig. 6 as bcc (which should be fcc). We thank Dr. E. Mele for checking and confirming this point.]

Removal of the dominant spherical charge density reveals significant differences between fcc and bcc copper as demonstrated in Fig. 3, which shows $\rho(\mathbf{r})-\rho_0(|\mathbf{r}|)$. The

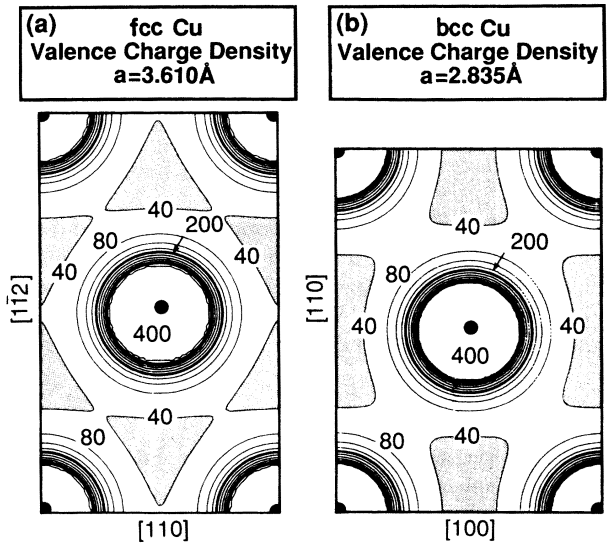

FIG. 2. Total valence-electron charge densities for (a) fcc Cu at the experimental equilibrium lattice constant and (b) bcc Cu at the calculated equilibrium lattice constant, as obtained from the present all-electron calculation. Shaded areas highlight the interstitial charge densities (contour levels 40×10^{-3} e/a.u.^{3} and below). Contour steps are 40×10^{-3} e/a.u.^{3} The high-density fluctuations within about 0.5 Å of the nuclear were removed from these plots for clarity.

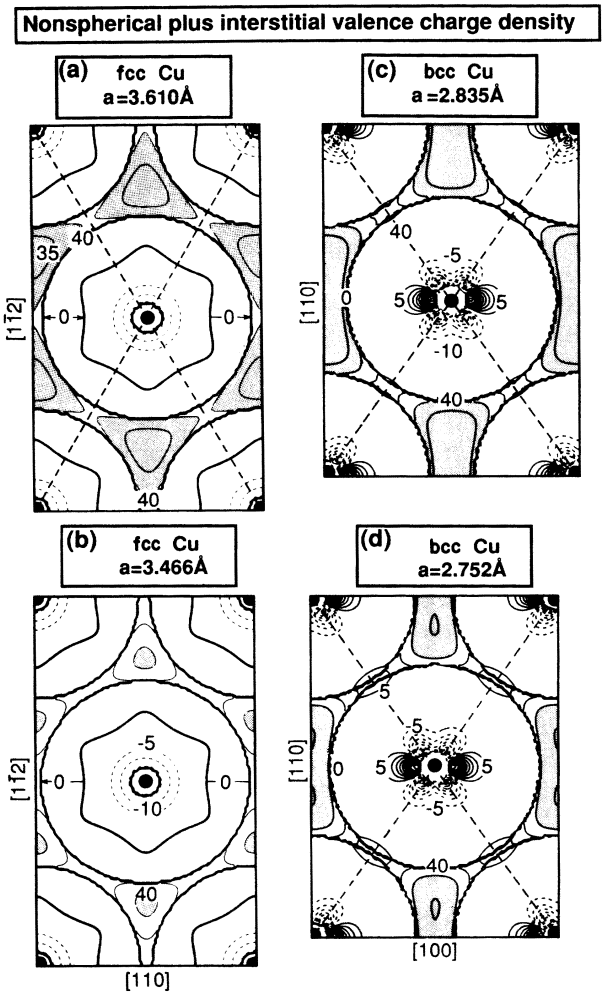

FIG. 3. Nonspherical and interstitial valence-electron charge densities $\rho(\mathbf{r})-\rho_0(\mathbf{r})$ [Eq. (1)] for fcc [(a) and (b)] and bcc [(c) and (d)] Cu. The shaded regions highlight the interstitial charge densities (contour levels 40×10^{-3} e/a.u.^{3} and below) calculated from Eq. (2). (a) fcc Cu, $a=3.610$ Å; (b) fcc Cu, $a=3.466$ Å; (c) bcc Cu, $a=2.835$ Å; (d) bcc Cu, $a=2.752$ Å. Solid (dashed) contours represent positive (negative) charge-density differences. The straight dashed lines in (a) and (b) denote the nearest-neighbor bond directions. Contour step: 5×10^{-3} e/a.u.^{3}

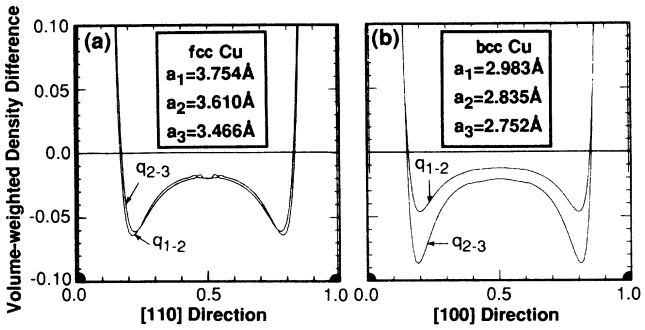

FIG. 4. Volume-weight valence-electron charge-density difference [Eq. (3)] for (a) fcc and (b) bcc Cu.

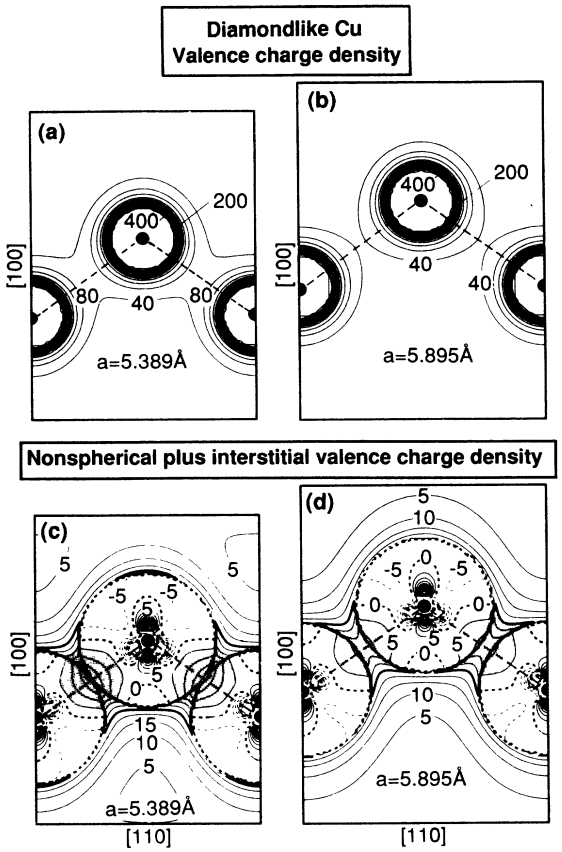

FIG. 5. Total valence-electron charge density [(a) and (b)] and nonspherical and interstitial charge density $\rho(\mathbf{r})-\rho_0(\mathbf{r})$ [(c) and (d)] for Cu in the diamond structure. The straight dashed lines in (a) and (b) denote the nearest-neighbor bonds. Solid (dashed) contours in (c) and (d) denote positive (negative) values. Contour steps are 40×10^{-3} e/a.u.^{3} in (a) and (b) and 5×10^{-3} e/a.u.^{3} in (c) and (d). In (a) and (b) we have removed the large density fluctuations within about 0.5 Å of the nuclei for clarity of display.

common features of $\rho_{NS}(\mathbf{r})$ in fcc and bcc Cu are the following. (i) The relative amplitude $\rho_{NS}(\mathbf{r})/\rho(\mathbf{r})$ of the nonspherical density with respect to the total valence-electron density are small in both cases, reflecting the nearly complete d^{10} shell and the full cubic symmetry in fcc and bcc Cu. Note that the nonspherical components are far smaller than the average valence-electron charge density ($11/V_0=0.139$ e/a.u.^{3} at the equilibrium fcc volume). (ii) The nonspherical density acts in both structures to remove charge from the nearest-neighbor Cu—Cu *bonds* (indicated in Fig. 3 by the straight dashed lines), depositing it in "nonbonding" regions *between atoms*. (iii) $\rho_{NS}(\mathbf{r})$ is localized near the atomic sites, and, hence, encompasses but a small fraction of the unit-cell volume. The obvious differences in ρ_{NS} of bcc and fcc Cu at their equilibrium volumes is that the bcc structure has larger nonspherical components than the fcc structure, and that these are differently oriented (reflecting differences in the coordination number: 12 for fcc and 8 for bcc). Since the lattice harmonics $K_l(\hat{\mathbf{r}})$ are common to the fcc and bcc lattices, these difference, reflect, by necessity, different radial weights $\rho_l(|\mathbf{r}|)$ for the various angular momenta (bcc copper has a larger $\rho_{l=4}$ than fcc copper).

To assess the *deformational* properties of the nonspherical charge densities, we show in Figs. 3(c) and 3(d) the nonspherical density $\rho_{NS}(\mathbf{r})$ in the MT spheres and $\rho(\mathbf{r})$ in the interstitial regions calculated at reduced lattice constants. In all cases shown in Fig. 3, we have shaded the interstitial contours corresponding to charge-density values of 40×10^{-3} e/a.u.^{3} to emphasize the way in which the interstitial density response to deformation (it obviously diminishes). We see that other than this change in the interstitial charge density, compression has

TABLE II. Calculated total energies plus 3302.0 Ry for fcc, bcc, and diamondlike Cu with and without the nonspherical charge-density components inside the MT spheres.

	Cu—Cu bond length (Å)	$E_{tot}(l_{max}=8)$ (Ry)	$E_{tot}(l_{max}=0)$ (Ry)	Difference (meV)
fcc ($a_{eq}=3.562$ Å)	2.519	−0.931 55	−0.931 53	−0.27
fcc ($a_{expt}=3.610$ Å)	2.553	−0.930 75	−0.930 80	+0.68
bcc ($a_{eq}=2.835$ Å)	2.455	−0.927 96	−0.927 86	−1.40
diamond ($a=5.895$ Å)	2.553	−0.801 11	−0.799 62	−20.3
diamond ($a=5.389$ Å)	2.334	−0.832 32	−0.827 62	−63.9

but a small effect on $\rho_{NS}(\mathbf{r})$: it is slightly enhanced at reduced volume. To amplify the visual effect of the response of the nonspherical charge to compression, we show in Fig. 4 the volume-weighted density difference suggested by KTMS,[1] i.e.,

$$q_{i-j}(\mathbf{r})=[\rho_i(\mathbf{r})\Omega_i-\rho_j(\mathbf{r})\Omega_j]/N\ , \tag{3}$$

where ρ_i and ρ_j are self-consistently calculated charge densities at the cell volume Ω_i and Ω_j, respectively, and $N=11$ is the number of valence electrons. The results for fcc [Fig. 4(a), plotted along the [110] direction] and bcc [Fig. 4(b), plotted along the [100] direction] copper show but a weak dependence of the nonspherical density on deformation: compression enhances ρ_{NS} just slightly. More importantly, these changes are found to be *monotonic* with the volume changes $\Omega_i-\Omega_j$. We conclude the following.

(i) ρ_{NS} at the equilibrium volumes of both fcc and bcc copper is small in amplitude and localized in a small volume *near the core*, and, hence, is unlikely to affect the structural preference energy $E_{bcc}-E_{fcc}$.

(ii) While ρ_{NS} increases upon compression (and is larger in bcc than in fcc copper), this increase is *monotonic* with compression in both systems.

To investigate these points, we have repeated the total-energy calculations self-consistently for fcc and bcc Cu at their respective equilibrium lattice constants, *omitting* the nonspherical pieces of the charge density and potential in the MT spheres. The results (Table II) show that the nonspherical pieces have but a negligible effect on the total energies (unchanged to within 1.4 meV) or on the structural energies $E_{bcc}-E_{fcc}$ (48.8 meV retaining ρ_{NS}, 49.9 meV without it). The calculated lattice constants and bulk moduli are practically the same as those obtained by retaining the full charge density. This is consistent with the success of band-structure methods which assume $\rho_{NS}=0$ inside the MT spheres[4-6] in correctly reproducing structural energies in close-packed metals. The double-well metastability found by KTMS in bcc Cu [Fig. 1(a)] is clearly not a consequence of the different response of ρ_{NS} in fcc and bcc copper to deformations.

It is obvious, however, that the success of methods omitting ρ_{NS} cannot be extended to *open structure:* To examine this we have self-consistently calculated the total energies of copper in the fourfold-coordinated diamondlike structure at two different volumes, using the same convergence parameters as in fcc and bcc Cu, and ten special-**k** points. Here, the nonspherical charge density lowers the total energies considerably more than in close-packed Cu: by 20.3 meV (30 times more than in fcc Cu at $a_{expt}=3.610$ Å), and by 63.9 meV at $a=5.389$ Å (a cell volume which is still 60% larger than the equilibrium fcc volume). As in fcc and bcc Cu, volume compression enhances the nonspherical charge density and its contribution to the total energy. Figure 5 depicts the total valence-electron charge densities $\rho(\mathbf{r})$ [Figs. 5(a) and 5(b)] and $\rho(\mathbf{r})-\rho_0(\mathbf{r})$ [Figs. 5(c) and 5(d)]. We see again that *near the core* ρ_{NS} acts to deposit charge in "nonbonding" regions *between* atoms. However, in the diamond structure, ρ_{NS} acts also to pile up charge on the Cu—Cu bond (shaded regions); this covalent charge buildup increases with decreasing volume (consistent with the fact that the contribution of ρ_{NS} to the total energy increases at smaller volumes).

We conclude that nonspherical densities exist in bcc, fcc, and diamondlike Cu, and that they increase with reduced coordination numbers and with reduced molar volumes. However, they have a negligible effect on fcc versus bcc structural energy differences in Cu (and a larger effect on diamondlike Cu); hence, they do not induce curvature changes or metastabilities in the total-energy curve.

ACKNOWLEDGMENTS

We thank Dr. S. Froyen and Dr. J. Bernard for assistance with the computer systems. This work was supported by the Office of Energy Research (OER), Division of Materials Sciences, The Office of Basic Energy Sciences (BES) of the U.S. Department of Energy, under Contract No. DE-AC02-77-CH00178.

[1] M. H. Kang, R. C. Tartar, E. J. Mele, and P. Soven, Phys. Rev. B **35**, 5457 (1987).

[2] P. Bendt and A. Zunger, Phys. Rev. B **26**, 3114 (1982).

[3] Lattice constants are taken from the *American Institute of Physics Handbook,* 3rd ed. (McGraw-Hill, New York, 1972), Table 9*d*-3; bulk moduli are taken from K. Geschneider, Jr., in *Solid State Physics,* edited by H. Ehrenreich, F. Seitz, and D. Turnbull (Academic, New York, 1964), Vol. 16; cohesive energies are taken from R. Hultgren, R. L. Orr, and K. K. Kelly, *Selected Values of Thermodynamic Properties of Metals and Alloys* (Wiley, New York, 1965); see also *Physical Acoustics,* edited by W. P. Mason (Academic, New York, 1965), Vol. III-B.

[4] V. L. Moruzzi, J. F. Janak, and A. R. Williams, *Calculated Electronic Properties of Metals* (Pergamon, New York, 1978).

[5] A. R. Williams, J. Kübler, and C. D. Gelatt, Phys. Rev. B **19**, 6094 (1979); P. M. Marcus, V. L. Moruzzi, Z. Q. Wang, Y. S. Li, and F. Jona, in *Physical and Chemical Properties of Thin Metals Overlayers and Alloy Surfaces,* Vol. 83 of *Materials Research Society Symposia Proceedings,* edited by D. M. Zehner and P. W. Goodman (Materials Research Society, Pittsburgh, PA, 1987).

[6] K. Terakura, T. Oguchi, T. Mohri, and K. Watanabe, Phys. Rev. B **35**, 2169 (1987).

[7] J. R. Chelikowsky and M. Y. Chou, Phys. Rev. B **38**, 7966 (1988).

[8] I. A. Morrison, M. H. Kang, and E. J. Mele, Phys. Rev. B **39**, 1575 (1989).

[9] S.-H. Wei, H. Krakauer, and M. Weinert, Phys. Rev. B **32**, 7792 (1985), and references therein.

[10] P. Hohenberg and W. Kohn, Phys. Rev. **136**, B836 (1964); W. Kohn and L. J. Sham, *ibid.* **140**, A1133 (1965).

[11] E. Wigner, Phys. Rev. **46**, 1002 (1934).

[12] H. J. Monkhorst and J. D. Pack, Phys. Rev. B **13**, 5188 (1976).

[13] S.-H. Wei, A. A. Mbaye, L. G. Ferreira, and A. Zunger, Phys. Rev. B **36**, 4163 (1987).

[14] D. M. Ceperley and B. J. Adler, Phys. Rev. Lett. **45**, 566 (1980).

[15] P. Perdew and A. Zunger, Phys. Rev. B **23**, 5408 (1981).

[16] L. Hedin and B. I. Lundqvist, J. Phys. C **4**, 2064 (1971).

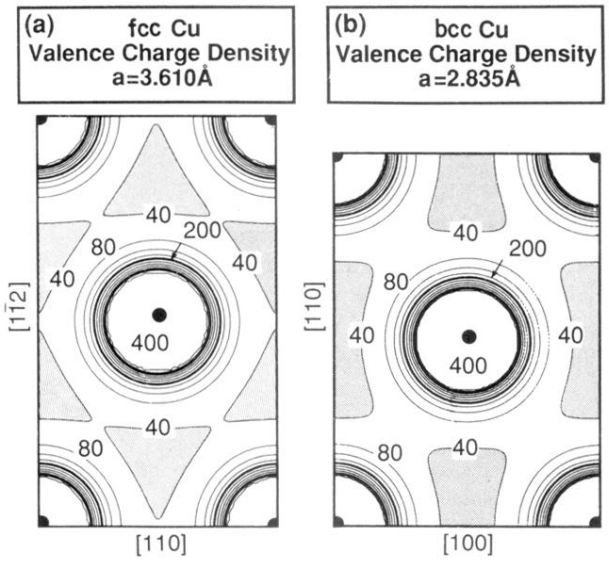

FIG. 2. Total valence-electron charge densities for (a) fcc Cu at the experimental equilibrium lattice constant and (b) bcc Cu at the calculated equilibrium lattice constant, as obtained from the present all-electron calculation. Shaded areas highlight the interstitial charge densities (contour levels 40×10^{-3} e/a.u.^{3} and below). Contour steps are 40×10^{-3} e/a.u.^{3} The high-density fluctuations within about 0.5 Å of the nuclear were removed from these plots for clarity.

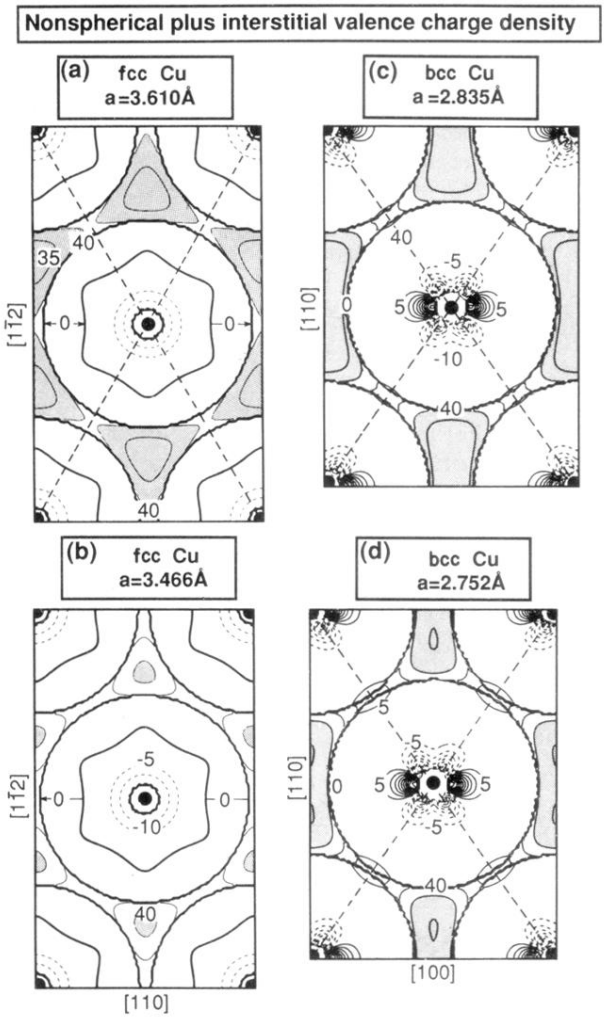

FIG. 3. Nonspherical and interstitial valence-electron charge densities $\rho(\mathbf{r})-\rho_0(\mathbf{r})$ [Eq. (1)] for fcc [(a) and (b)] and bcc [(c) and (d)] Cu. The shaded regions highlight the interstitial charge densities (contour levels 40×10^{-3} e/a.u.^{3} and below) calculated from Eq. (2). (a) fcc Cu, $a=3.610$ Å; (b) fcc Cu, $a=3.466$ Å; (c) bcc Cu, $a=2.835$ Å; (d) bcc Cu, $a=2.752$ Å. Solid (dashed) contours represent positive (negative) charge-density differences. The straight dashed lines in (a) and (b) denote the nearest-neighbor bond directions. Contour step: 5×10^{-3} e/a.u.^{3}

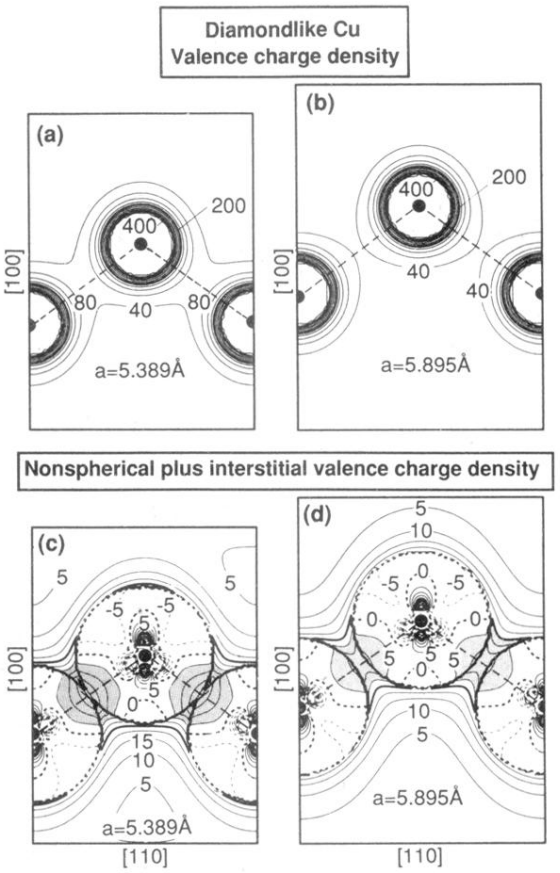

FIG. 5. Total valence-electron charge density [(a) and (b)] and nonspherical and interstitial charge density $\rho(\mathbf{r})-\rho_0(\mathbf{r})$ [(c) and (d)] for Cu in the diamond structure. The straight dashed lines in (a) and (b) denote the nearest-neighbor bonds. Solid (dashed) contours in (c) and (d) denote positive (negative) values. Contour steps are 40×10^{-3} e/a.u.^{3} in (a) and (b) and 5×10^{-3} e/a.u.^{3} in (c) and (d). In (a) and (b) we have removed the large density fluctuations within about 0.5 Å of the nuclei for clarity of display.